Anisotropic growth of long isolated graphene ribbons on the C face of graphite-capped *6H*-SiC

Nicolas Camara,[1,*] Jean-Roch Huntzinger,[2,†] Gemma Rius,[1,‡] Antoine Tiberj,[2,§] Narcis Mestres,[3,‖]
Francesc Pérez-Murano,[1,¶] Philippe Godignon,[1,**] and Jean Camassel[2,††]

[1]*IMB-CNM-CSIC, Campus UAB, Bellaterra, Barcelona 08193, Spain*
[2]*GES, UMR-CNRS 5650, Université Montpellier 2, 34095 Montpellier Cedex 5, France*
[3]*ICMAB-CSIC, Campus UAB, Bellaterra, Barcelona 08193, Spain*

Using a graphite cap to cover the silicon carbide (SiC) sample, it is shown that large isolated graphene anisotropic ribbons can be grown on the C face of on-axis, semi-insulating, 6*H*-SiC wafers. The role of the cap is to modify the physics of the surface reconstruction process during Si sublimation, making more efficient the reconstruction of few selected terraces with respect to the others. The net result is the formation of a strongly step-bunched morphology with, in between, long (up to 600 μm) and large (up to 5 μm) homogeneous monolayers of graphene ribbons. This is shown by optical and scanning electron microscopy, while a closer view is provided by atomic force microscopy (AFM). From Raman spectroscopy, it is shown that most of the ribbons are homogeneous monolayers or bilayers of graphene. It is also shown that most of the thermal stress between the graphene layer and the 6*H*-SiC substrate is relaxed by wrinkles. The wrinkles can be easily displaced by an AFM tip, which demonstrates evidence of graphene ironing at the nanoscale. Finally and despite the very low optical absorption of a single graphene layer, one shows that differential optical microtransmission can be combined to the micro-Raman analysis to confirm the monolayer character of the thinnest ribbons.

I. INTRODUCTION

Graphene has emerged recently as a new material with outstanding electronic properties. This includes massless Dirac fermions, ballistic transport properties at room temperature, and good compatibility with the silicon planar technology.[1,2] Graphene-based devices are thus promising candidates to complement silicon in the future generations of high frequency microelectronic devices.[3] Different techniques have been developed over the past five years to fabricate monolayer or bilayer of graphene. They range from exfoliated graphite, either mechanically[1] or in a liquid-phase solution,[4] to chemical vapor deposition on a metal surface[5–8] and also to substrate-free synthesis when passing ethanol into an argon plasma.[9] Of course, for technical applications uniform growth of graphene on an insulating substrate is mandatory. Standard exfoliation of graphene from a graphite piece yields high quality crystals, but such isolated samples with dimensions in the 10–100 μm^2 range remain unsuitable for large-scale device production. The method investigated in this work consists of a controlled sublimation of few atomic layers of Si from a single crystal SiC substrate.[2] Such an epitaxial growth (EG) of graphene provides a homogeneous coverage of few monolayer graphene (MLG) on the full wafer surface[10–12] and seems today the most suitable option to meet the "more than Moore" requirements for the future electronic industry. An alternative to the full coverage of FLG is the discrete growth of graphene ribbons that can be easily interconnected. Toward this end, the selective EG of few layer graphene (FLG) in a narrow prepatterned area, like an opened window in an AlN mask deposited on a SiC substrate, has already been demonstrated.[13] This kind of growth on a bare SiC surface, without specific surface preparation patterning, can be achieved, with even more homogeneous results. It will be demonstrated in this work.

Basically, on both the Si and C faces of any SiC substrate, graphene grows selectively on some reconstructed parts of the surface. Controlling the growth means then controlling *locally* the surface reconstruction. At low pressure conditions, i.e., from ultrahigh vacuum (below 10^{-9} Torr) to standard secondary vacuum (SV) (in the range of 10^{-8}–10^{-6} Torr), it remains challenging to grow FLG on the Si face with homogeneous domain size larger than few hundred nanometers.[14–16] Low pressure sublimation from the C face leads to wider domains (and higher mobility) than the sublimation from the Si face,[15] but still, to increase homogeneity one has to lower the sublimation rate. This can be done by working at high pressure under a noble gas atmosphere. For the Si face this was done independently by Virojanadara *et al.* in Linköping[11] and by Emtsev *et al.* in Erlangen.[12] Performing graphitization on the Si face of a 6*H*-SiC substrate under argon at 900 mbar, both groups showed that one can get large homogeneous graphene monolayers and bilayers on top of the usual $(6\sqrt{3} \times 6\sqrt{3})R30°$ reconstructed parts of the (0001) SiC terraces. It seems very promising and probably opens an avenue for graphene-based electronics.

Unfortunately, some problems remain. On such Si faces, the first graphitic layer to be formed is a carbon-rich layer, made of sp^2 and sp^3 hybridized carbon atoms.[17,18] It appears in between the SiC substrate and the first "real" graphene layer and since this first graphene layer is strongly coupled to the SiC substrate, it drastically lowers the electronic mobility of carriers which does not exceed 2.000 cm^{-2} V^{-1} s^{-1} at low temperature.[12] On the opposite, on the **C**-face mobility values up to 27.000 cm^{-2} V^{-1} s^{-1} have been reported on FLG-based devices[19] and 250 000 cm^2 V^{-1} s^{-1} by noncontact optical methods on very similar FLG sheets.[20] Such outstanding values come because there is no "buffer" layer on the **C** face between the SiC substrate and the first graphene plane. This makes the top graphene layer very

similar to prototype (exfoliated) material.[17,21]

Since it is extremely difficult to grow a homogeneous MLG sheet on the C face of a 6*H*- or 4*H*-SiC substrate,[22] it is difficult to expect a homogeneous yield in device production at the full wafer scale. In this work, instead of studying turbostratic FLG sheets that look (more or less) like graphene, we propose to work directly with single, isolated, MLG of sizable dimension that can be easily interconnected or processed to make classical field-effect transistors or sensor devices.

In the first part of the paper, we demonstrate an innovative way to grow large (few thousand μm^2) homogeneous (isolated) monolayer or bilayer graphene ribbons on the C face of a semi-insulating SiC sample. In the second part, we focus on the investigation of the optical properties, including the answer to a frequently asked question: "How to be sure that one really deals with a single uniform MLG sheet?"

II. GROWTH TECHNOLOGY

All substrates were 1×1 cm^2 templates cut from a 3 in., on-axis, semi-insulating 6*H*-SiC wafer from Cree. Before cutting, electrochemical polishing was done by Novasic to get Epiready® morphology.[23] A sacrificial oxide was then thermally grown and chemically etched in HF to remove any (small) subsurface damage from the polishing process. All necessary chemical treatments were clean-room compatible and very similar to the ones used before thermal oxidation or postimplantation annealing in standard SiC technology. Atomically flat surfaces were obtained in this way. The impact of this preparation process on the final product is essential since it allows getting large and uniform terraces before starting the growth. The vacuum limit in the rf furnace was 10^{-6} Torr and, before sublimation, the samples were heated at 1150 °C for 10 min in order to remove any trace of native oxide. To demonstrate the benefic influence of the graphite cap, two series of samples from the same wafer were grown in two different ways. Samples from series A were grown without capping. Samples from series B were grown with a graphite cap on top.

III. RESULTS

Samples A were grown at 1550 °C for 5 min under SV. As already known, such growth conditions allow the formation of FLG flakes covering the whole SiC surface, but the flakes are not homogeneous.[10,22,24] This is because the starting point of the process (sublimation) is not at all intrinsic. Defects such as threading dislocations localize the process,[22] leaving behind a surface with inhomogeneous graphene flakes on top. If the sublimation temperature is elevated enough, the growth may start also between the defects. In this case, using optical microscope (OM) techniques in the cross-polarization mode [Fig. 1(a)] and the dark field mode [Fig. 1(b)], one easily evidences the growth features associated with the two different processes: (i) defect activated and (ii) more intrinsic nucleation.

In Fig. 1(a) we display the result of the fast growth of tens of graphene layer thick flakes nucleated around dislocations
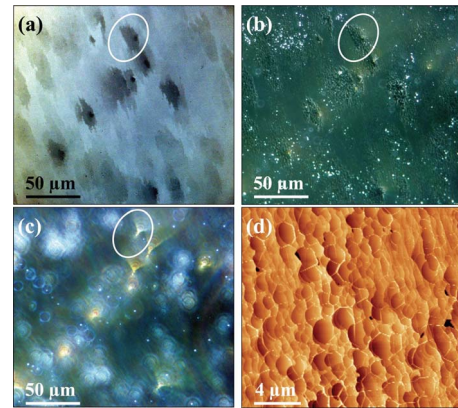

FIG. 1. (Color online) (a) Wide range crossed-polarization OM images of a sample from series A, fully covered with FLG. Growth conditions: temperature of 1550 °C, SV, no graphite cap. Thicker FLG areas appear darker as shown inside the white circle; (b) same area but in dark field mode. The OM image shows yellow dislocation spots that are at the origin of the thicker FLG; (c) same as (b) except for a slight defocusing which allows a better localization of dislocations; and (d) AFM image taken in the gray sea area in between the thick FLG.

from the SiC substrate. These dislocations are best seen in the dark field mode in Fig. 1(b), in which they appear as yellow spots located at the center of the thicker flakes. For clarity, a typical example is shown in the white circle. Defocusing the microscope a few microns below the sample surface, these spots become even more visible, appearing now as yellow cones in Fig. 1(c). Finally, surrounding the darker and/or thicker areas are thinner FLGs which form a "gray sea," already discussed in the work in Ref. 22. In the following, this more intrinsic (but less performing) formation process will be called "gray sea process." It results in the atomic force microscopy (AFM) flake structure shown in Fig. 1(d), with an average domain size which hardly reaches 1 μm diameter.[25,26] Altogether, such a growth process is not at all expected to produce a large and homogeneous pavement, with a single uniform MLG sheet covering the whole SiC wafer. To meet that goal, a new and radically different growth process has been developed.

The main idea was to quench the gray sea process rather than optimizing it. To this end, we focused on the control of the defect-assisted growth. This was done on samples from series B by covering the surface with a graphite cap. Capping is not new in SiC process technology. It constitutes a well known technique for postimplantation annealing and was used for years on Al-implanted SiC wafers.[27] In this case, most of the time the cap was a simple layer of spin-deposited and baked photoresist. In this work, the graphite cap did not need to be so tightly bound and we only used a wafer of graphite put on the SiC surface. Since the cap and the SiC sample did not stick together during the growth, there was no need for a particular procedure to separate them at the end of process. We have found the following:

(i) Increasing the C and Si partial pressures over the SiC surface, the graphite cap lowers the Si out-diffusion process. At ~1550 °C this resulted in a complete quenching of any graphitic material growth.
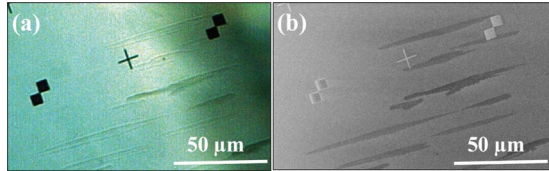
FIG. 2. (Color online) (a) OM image in the Nomarski crossed polarization mode of the large graphene ribbons grown at 1700 °C on a sample covered with a graphite cap; (b) SEM image of the same area. The graphene ribbons appear light gray, while a thick multilayer is slightly darker. Notice that most of the graphene ribbons of (b) do not resolve at all on (a) indicating in most cases not more than one or two layers of graphene (controlled by micro-Raman). The crosses and squares are deposited gold marks.

(ii) Raising the temperature to 1700 °C, the gray sea remained quenched while long graphene ribbons appeared. They were up to 5 μm wide and 100 μm long for a 15 min process. Constantly the ribbons are surrounded by graphene free SiC areas. Typical ribbons are shown in the Nomarski crossed polarization OM mode and by scanning electron microscopy (SEM) images of Fig. 2.

(iii) Thanks to OM investigation in dark field mode, we can see that dislocations are still presently seen as yellow cones in Fig. 3. Time to time they are the center of the ribbon and act as an efficient nucleation centers as shown on the ribbon from Fig. 3(a). In many cases, a ribbon exists without any identified defect at the origin, but it was found that a higher density of extrinsic defects such as scratches, dust, or other particles induces a higher (local) density of ribbons as shown on the top right image of Fig. 3(b) taken on the same sample as Fig. 3(a).
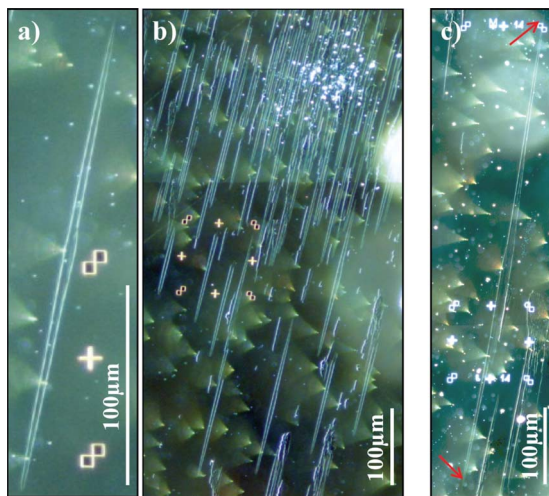

FIG. 3. (Color online) (a) and (b) OM images collected at different magnifications in dark field mode for a sample from series B, annealed at 1700 °C during 30 min under SV but covered with a graphite cap. A large part of the 6H-SiC surface is covered by 50–250-μm-long graphene ribbons all oriented parallel. In such growth, defects such as the dislocation in the center of the ribbon in (a) or contamination dust like in the top right corner of (b) can act both as nucleation centers. (c) For a higher processing time, longer ribbons have been obtained in the range of 600 μm when annealed during 60 min. The red arrows indicate the extremities of the graphene ribbon.
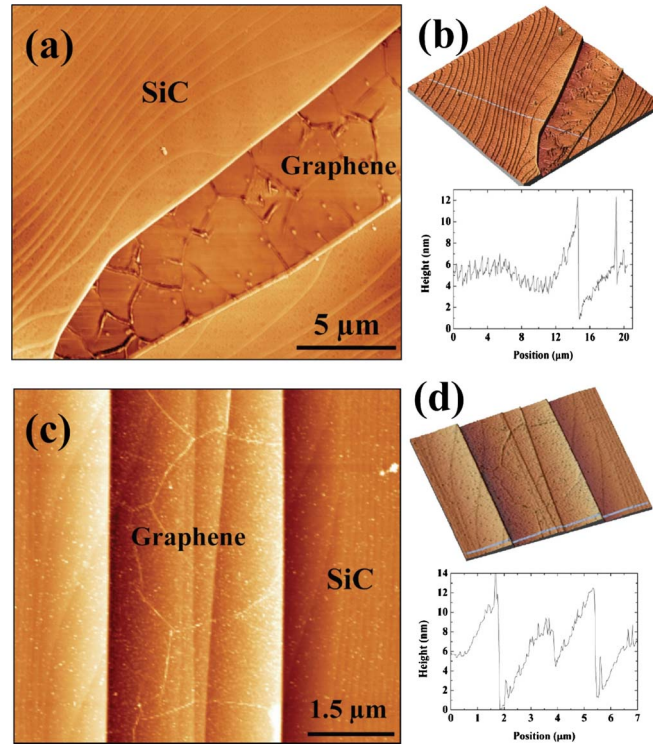

FIG. 4. (Color online) (a)–(d) AFM pictures of two different graphene monolayers. Around the ribbon is strong SiC step bunching. (a) Wide range view of the phase mode and (b) the associated three-dimensional AFM topography with profile. (c) Higher magnification in topography mode of another monolayer ribbon and (d) its associated 3D image and profile. Notice the strong SiC step bunching in the 10 nm range when a terrace with graphene on top. A more standard 1–2 nm step is measured when the SiC surface has not been converted into graphene.

(iv) The longer the graphitization process lasts, the longer the ribbons are. Indeed, while the ribbons coming from Fig. 2 annealed during 15 min hardly reach 100 μm, it is shown on the OM pictures of Figs. 3(a) and 3(b) that the ribbons created by a 30 min annealing process are much longer, up to 250 μm. When increasing even more the process time, up to 1 h, some ribbons are as long as 600 μm [Fig. 3(c)].

(v) Before graphene growth, the SiC surface reorganizes itself to form long and large terraces. This is shown on the series of AFM pictures displayed in Fig. 4. Notice however that only the larger terraces exhibit a graphene ribbon on top. Adjacent to these large terraces with graphene on top are very high steps, which are clearly seen on the three-dimensional (3D) AFM profiles. They can be more than 10 nm high and come from the step-bunching mechanism that usually accompanies the enlargement process.[28]

IV. DISCUSSION

At the beginning of the growth process all terraces had the same nominal width $W_N \sim 800$ nm, as can be estimated from the unreconstructed part of surface shown in the AFM profile of Fig. 4(b). This is only function of the miscut angle θ. All steps had also the same height (~ 1.5 nm or one 6H unit

cell). Increasing the temperature, at some points on the wafer, specifically where a "defect" is present, the step-bunching process is disturbed and two or more original terraces started to merge, defining new enlarged terraces with higher step edges until in some part of the enlarged terraces with higher step edges the critical width for surface reconstruction (W_c) was reached. Then, on these parts of terraces, surface reconstruction started.

Surface reconstruction is a well-known process (at least for the ⟨111⟩ reconstructed 7×7 surface of silicon[28,29]) which *lowers* the free surface energy per unit area (f) by Δf. But at the same time, it *increases* the free energy cost per unit length for edge step formation (β) by $\Delta \beta$. This is the basic reason why a critical width (W_c) is needed for surface reconstruction, such that

$$W_c > \Delta \beta / |\Delta f|.$$

Once this condition has been met in some part of a terrace, reconstruction (2×2 or 3×3 on the C face of on-axis $6H$-SiC) expands rapidly, enlarging at the same time the terrace width and the step height. At the same time during the surface reconstruction process and on the enlarged and reconstructed (2×2 or 3×3) terraces, the original defect nucleates into graphene seed and expands. The net result is that the growth of graphene lowers the energy of incorporated carbon atoms. This is the driving force that makes all free carbon atoms around (and, of course, within a distance lower than the surface diffusion length) to incorporate in that part of terrace. This basic mechanism could explain the selection of a given terrace.

Once a seed has been formed, the mixed process of surface reconstruction with graphene on top changes the free surface energy and the energy for step edge formation, resulting in a larger value of the critical width W_c. It stabilizes the terrace where the graphene growth expands rapidly along it, increasing its width and bunching more steps. The final value of step height (~10 nm) suggests that at least five nominal terraces had to merge together in order to constitute the final template for the large graphene ribbon. Of course, since all reconstructed terraces remain parallel to the original (11–20) step direction, all graphene ribbons grow parallel only confined between the two edges of a terrace. This explains the (apparent) growth anisotropy and the (unusual) length of ribbons.

The higher the annealing time, the longer the ribbons but no detailed statistics have been done yet. Simply, the 600 μm ribbon shown in Fig. 3(c) was found on a sample that has been sublimated twice longer than the sample with the 250 μm ribbons shown in Figs. 3(a) and 3(b) and four times longer than the sample with the 100 μm ribbons shown in Fig. 2. This confirms the model of the localized original nucleation center rather than the model of the nucleation from the edge of terrace as in the case of the Si face.[12]

Opposite to graphene exfoliated on a 300-nm-thick SiO_2 film on Si wafer, thin epitaxial graphene layers on SiC substrate are almost invisible by OM in the standard reflection mode.[30] This is clear from the comparison of Figs. 2(a) and 2(b). What is actually seen in Figs. 2 and 3 by OM are the bunched steps at the edge of invisible ribbons. This is simply
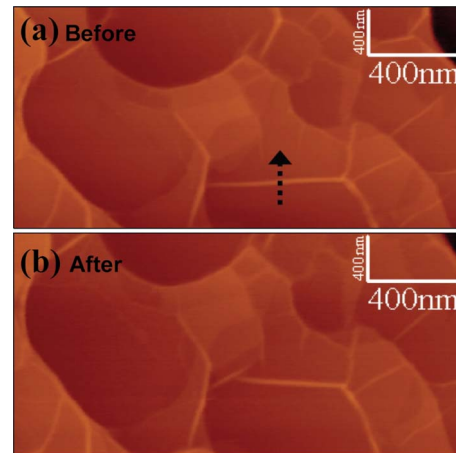

FIG. 5. (Color online) Example of ironing FLG at the nanoscale. (a) AFM picture taken before moving the wrinkle with an AFM tip in contact mode. The trajectory of the AFM tip to displace the wrinkle is highlighted by the black arrow. (b) AFM picture after the graphene being ironed. The wrinkle is displaced by about 100 nm.

because the crossed polarized Nomarski mode and the dark field mode enhance the resolution of scattered light at the step edges.

From AFM, we find that most of these "invisible" graphene ribbons are atomically flat, exhibiting only wrinkles as usually found for graphitic material grown on SiC.[25] These wrinkles are few nanometers high and have a rough trigonal structure. This is best seen in the AFM pictures of Fig. 4. Since the thermal expansion coefficient of SiC is larger than the one of graphene, the resulting thermal stress should be large and compressive. On the C face of SiC and because of the weak interaction between the substrate and graphene layer(s), the stress relaxes through the formation of wrinkles. In our case, large, atomically flat and wrinkle-free areas exist in the range of several μm^2. Even if necessary, these areas can be increased by "ironing" the wrinkles at the nanoscale. To this end, as shown in Fig. 5 in the case of FLG, the tip of the AFM probe in contact mode is enough due to the weak interaction between the graphene ribbon and the underlying substrate.

To summarize, at the end of the process, long isolated graphene ribbons occupy most of the time one single terrace, surrounded by sharp and high edges. The fact than most of the time, only one terrace is affected by the growth could be explained by two main reasons: (i) the neighboring terraces width is lower than the critical value W_c, no surface reconstruction appears and by consequences no graphene grows; (ii) the steps are so high between the reconstructed terrace and the neighbors that it is energetically less expensive for the C atoms to stay on the same initial terrace. This stops the graphene growth perpendicular to the long direction of terraces. In some cases, two or three large terraces can merge [as shown in Fig. 4(c)] showing some weaker steps in between. This suggests that, when the steps are small enough, the graphene growth can happen on the neighboring terraces. Thus, by using other substrates with different miscut of the initial wafer, we assume that larger graphene ribbons can be expected.
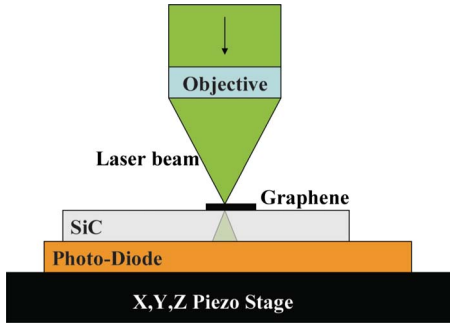
FIG. 6. (Color online) Schematic setup of the mixed techniques: micro-Raman and micro-optical transmission.

Furthermore, at the present time, the process is mainly dependent on uncontrolled reconstruction and seeding factors. But there is still much room for improvement to control the process. One can think to reduce the number of initial SiC surface defects by a high quality homoepitaxy growth and to perform proper local surface engineering treatments to initiate the nucleation (nanoscratches by an AFM tip, etching of trenches in the SiC surface, controlled deposition of nanoparticles on the surface, etc.).

V. OPTICAL INVESTIGATION TOOLS

Since the graphene overlayers on SiC are hardly visible by bright field optical microscopy, we know already that most of the growth product is less than five layer thick. Of course this is only indicative. To investigate in more detail the quality and thickness uniformity of the graphene ribbons, we combined micro-Raman spectroscopy with microtransmission measurements.

To perform simultaneously microtransmission measurement and Raman spectroscopy, we used a very simple technique, inserting a low noise photodiode between the SiC substrate and the XYZ piezoelectric stage (Fig. 6). It was then possible to measure at the same time and during the acquisition of Raman spectra, using the same laser beam as a probe, the power transmitted through the sample.

Then we were able to detect a relative power change in the range of few μW (for an incident power of ~ 1 mW) as the laser moved from a bare SiC area to a MLG ribbon and back. This technique is perfect for transparent SiC substrates but, of course, is not relevant for the opaque oxidized silicon substrates often used in graphene studies. Raman spectra were collected at room temperature using a Jobin Yvon-Horiba T64000 spectrometer in the confocal mode, with a $\times 100$ microscope objective. The 514 nm line of an Ar-Kr ion-laser was used for excitation. The spot size was ~ 1 μm. As usual, the bare SiC reference signal has been subtracted from experimental spectra.

We used this original technique to perform a 20 $\times 100$ μm^2 mapping of two neighboring graphene ribbons with a step size of 0.5 μm in X and 2 μm in Y (Fig. 7). The first map [Fig. 7(a)] corresponds to the transmitted power, the second [Fig. 7(c)] to the integrated intensity of the G band, and the third [Fig. 7(d)] 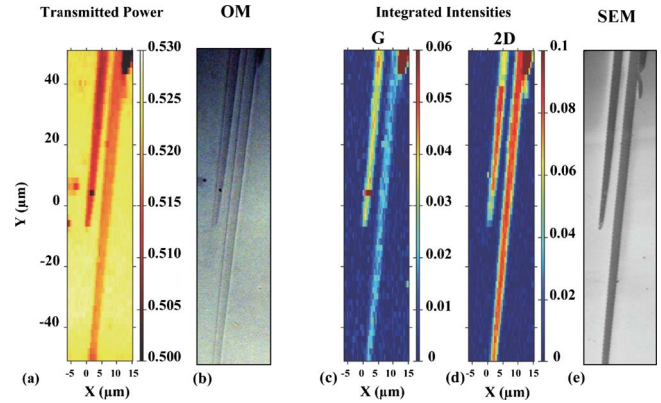to the integrated intensity of the 2D band. Because of the limited range of the XY piezostage (100×100 μm^2) the two ribbons could not be completely probed. The transmission map shows that both ribbons have excellent thickness uniformity. The left ribbon has a weaker transmitted power and hence is thicker than the right one.

FIG. 7. (Color online) 20×100 μm^2 mappings of two graphene ribbons grown on C-face $6H$-SiC with a graphite cap. The step sizes are 0.5 and 2 μm for the X and Y axes, respectively. (a) Power transmitted through the sample, detected by the photodiode as shown in Fig. 6, in arbitrary units. (b) is an optical microscopy of the same area. (c) and (d) Integrated intensities of the G and 2D Raman bands (defined in Fig. 8). (e) is the SEM image of the mapped area.

The transmittance of a graphene layer on top of a dielectric substrate has already been calculated.[31] The point is to consider a single interface between two media (for instance air and substrate) with boundary conditions for the electromagnetic field that are modified by the presence of the conducting graphene layer. In our case, the electrical permittivities of the two media are $\varepsilon_1 = 1.0$ and $\varepsilon_2 = 7.20$ for air and SiC substrate, respectively. The optical conductivity of a graphene monolayer is $\sigma = e^2/4\hbar$.[31] This prediction has been confirmed from transmission measurement through suspended monolayer graphene.[32] It leads to $T = 0.7814$ while without graphene (bare SiC substrate) the transmittance is $T_0 = 0.7912$. The corresponding relative extinction $\eta = (T_0 - T)/T_0$ is then theoretically 1.23% for a graphene monolayer. A bilayer has an optical conductivity twice as large as a monolayer in the visible range[33] leading to a relative extinction of 2.44%. Of course, the actual transmittance of the sample depends also on the back side SiC/air interface, which is optically polished in our case. Nevertheless, this simply involves a common factor that cancels out, so that η depends only on the relative change in the transmittance through the first interface.

From the transmission map and additional point by point measurements, we found that the right ribbon has a relative extinction η between 1.2% and 1.4%, confirming without any ambiguity that it is a true MLG ribbon. We notice also the good agreement with the theoretical predictions. A typical Raman spectrum measured at the center of ribbon is shown in Fig. 8. As a matter of fact, all spectra taken on this ribbon were almost identical, with a Raman fingerprint very close to the ones found in the literature for monolayers of
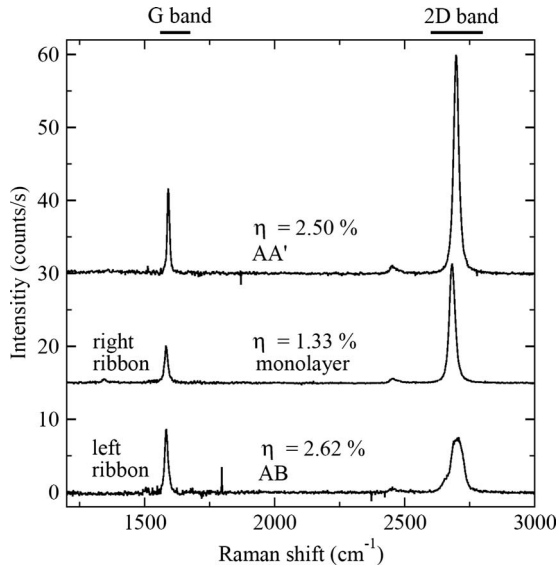
FIG. 8. Raman spectra acquired in the middle of different graphene ribbons, with the corresponding relative extinction $\eta = \Delta T/T_0$. From top to bottom: a misoriented bilayer (AA′), a monolayer, and a Bernal stacked bilayer (AB). The monolayer and the AB bilayer come from the right and left ribbons visible in Fig. 7, respectively. The G band and 2D band ranges used to extract the integrated intensities of Fig. 7 are shown above the figure.
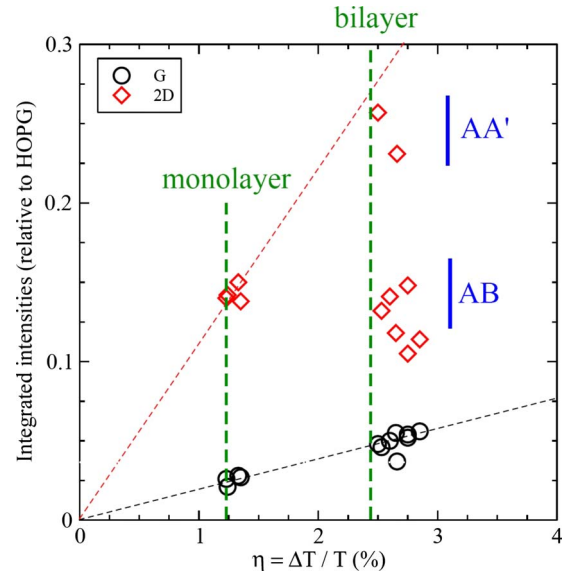

FIG. 9. (Color online) Plot of the integrated intensities of the G and 2D Raman bands (defined in Fig. 8), against the relative extinction $\eta = \Delta T/T_0$, i.e., the relative change in the transmitted power between the graphene ribbon and a bare SiC area nearby. The green vertical dashed lines show the theoretical values for monolayers and bilayers on SiC. The other dashed lines are only guide for the eyes.

exfoliated graphene on top of a SiO_2/Si substrate.[34–40]

The 2D band has a single Lorentzian line shape centered at 2685 ± 3 cm^{-1} while the full width at half maximum (FWHM) is below 25 cm^{-1}. The G band falls between 1583 and 1587 cm^{-1}, with a FWHM in the order of 13 cm^{-1}. The ratio of integrated intensities I_{2D}/I_G for the MLG ranges from 5 to 8. The most striking point is that the 2D and G bands are not significantly shifted to high frequency with respect to exfoliated graphene. This is an important difference with many previous works dealing with EG on the Si face of SiC wafers where a high thermal stress has been observed.[41–43] In our case, this stress has been relaxed by the formation of the wrinkles seen by AFM in Fig. 3. This stress relaxation has been observed on all the samples grown in the same conditions. Altogether with the fact that we have almost no D band, these observations suggest the growth of a high quality and basically strain relaxed graphene layers.

The second ribbon (on the left) has a relative extinction η between 2.6% and 2.8%, which corresponds to a bilayer. While the transmission and G band integrated intensity maps indicate a good thickness uniformity (Fig. 6), its Raman spectrum, marked as AB in Fig. 8, is typical of Bernal stacking.[34] Notice that this result is not systematic. On some other ribbons (not shown) we have found evidence of misorientation: the peak remains narrow, but it is twice intense than the one collected on the MLG. One of these spectra is shown as AA′ in Fig. 7.

Concerning the decrease in the 2D band intensity at the top 10 μm and at the bottom 10 μm in Fig. 7(d), a clear explanation is still missing. Nevertheless, it seems related to the defects identified by SEM in Fig. 7(e).

We summarize all results obtained on these ribbons on Fig. 9, plotting the integrated intensities of the G and 2D

bands against the corresponding relative extinctions η. The theoretical predictions for η are shown as vertical dashed lines for monolayer and bilayer graphenes. A clear correlation exists between the integrated intensity of the G band and the extinction. However and despite this correlation, the scattering of the G band intensity is too large to be used as an absolute thickness measurement.

It constitutes a first guess but cannot discriminate without any ambiguity between a monolayer and a bilayer. In the same way, the 2D band intensity can definitely not be used alone. As a matter of fact a Bernal stacked bilayer (marked as AB in Fig. 8) is just as intense as a monolayer. On the other hand, we have found several times bilayer ribbons with the same Raman shape as a monolayer. Simply they give a Raman signal twice as intense (marked as AA′ in Figs. 7 and 8). As already said, this corresponds to misoriented bilayer graphene predicted in Ref. 44 and already reported for exfoliated graphene on SiO_2/Si.[45,46] It might be tempting to conclude that a combination of 2D band intensity and shape would give the right answer, but even the 2D band intensity can fluctuate, depending on the doping level for instance.[37,40] Transmission measurements give good results, of course provided impurities on the graphene layer or on the bare SiC reference area are avoided. Finally, we think that combined measurement and analysis of the transmission and of the Raman shape and intensities are the best way to ascertain the monolayer character of a particular graphene flake.

VI. CONCLUSION

Working at high temperature (~ 1700 °C) with a graphite cap to lower the sublimation of Si species, we have shown that long, homogeneous, graphene ribbons could be grown

on the C face of a SiC wafer. The longest ones were 600 μm long and 5 μm wide. All were oriented in the same direction, with wrinkle-free areas of several μm^2. Combining AFM, optical microscopy, and SEM, we have shown that these ribbons fully occupy a single terrace of the reconstructed, step-bunched, SiC surface. Raman spectroscopy indicates high quality, slightly strained, homogeneous ribbons. A standard Raman spectrum of a graphene monolayer epitaxied on the C face of a SiC wafer was presented. In addition, we have shown that optical differential transmission is an easy and successfully tool to prove the monolayer character of ribbons. When working on transparent substrates such as SiC, we expect this technique to spread widely as a companion tool for Raman.

*nicolas.camara@imb-cnm.csic.es

†jean-roch.huntzinger@univ-montp2.fr

‡gemma.rius@imb-cnm.csic.es

§antoine.tiberj@ges.univ-montp2.fr

∥narcis.mestres@icmab.es

¶francesc.perez@imb-cnm.csic.es

**philippe.godignon@imb-cnm.csic.es

††jean.camassel@ges.univ-montp2.fr

[1] K. S. Novoselov, A. K. Geim, S. V. Morozov, D. Jiang, M. I. Katsnelson, I. V. Grigorieva, S. V. Dubonos, and A. A. Firsov, Nature (London) **438**, 197 (2005).

[2] C. Berger, Z. M. Song, T. B. Li, X. B. Li, A. Y. Ogbazghi, R. Feng, Z. T. Dai, A. N. Marchenkov, E. H. Conrad, P. N. First, and W. A. de Heer, J. Phys. Chem. B **108**, 19912 (2004).

[3] P. Sutter, Nature Mater. **8**, 171 (2009).

[4] Y. Hernandez, V. Nicolosi, M. Lotya, F. M. Blighe, Z. Sun, S. De, I. T. McGovern, B. Holland, M. Byrne, Y. K. Gun'Ko, J. J. Boland, P. Niraj, G. Duesberg, S. Krishnamurthy, R. Goodhue, J. Hutchison, V. Scardaci, A. C. Ferrari, and J. N. Coleman, Nat. Nanotechnol. **3**, 563 (2008).

[5] P. W. Sutter, J. I. Flege, and E. A. Sutter, Nature Mater. **7**, 406 (2008).

[6] J. Coraux, A. T. N'Diaye, C. Busse, and T. Michely, Nano Lett. **8**, 565 (2008).

[7] K. S. Kim, Y. Zhao, H. Jang, S. Y. Lee, J. M. Kim, K. S. Kim, J. H. Ahn, P. Kim, J. Y. Choi, and B. H. Hong, Nature (London) **457**, 706 (2009).

[8] X. S. Li, W. W. Cai, J. H. An, S. Kim, J. Nah, D. X. Yang, R. Piner, A. Velamakanni, I. Jung, E. Tutuc, S. K. Banerjee, L. Colombo, and R. S. Ruoff, Science **324**, 1312 (2009).

[9] A. Dato, V. Radmilovic, Z. H. Lee, J. Phillips, and M. Frenklach, Nano Lett. **8**, 2012 (2008).

[10] J. Kedzierski, P. L. Hsu, P. Healey, P. W. Wyatt, C. L. Keast, M. Sprinkle, C. Berger, and W. A. de Heer, IEEE Trans. Electron Devices **55**, 2078 (2008).

[11] C. Virojanadara, M. Syvajarvi, R. Yakimova, L. I. Johansson, A. A. Zakharov, and T. Balasubramanian, Phys. Rev. B **78**, 245403 (2008).

[12] K. V. Emtsev, A. Bostwick, K. Horn, J. Jobst, G. L. Kellogg, L. Ley, J. L. McChesney, T. Ohta, S. A. Reshanov, J. Rohrl, E. Rotenberg, A. K. Schmid, D. Waldmann, H. B. Weber, and T. Seyller, Nature Mater. **8**, 203 (2009).

[13] N. Camara, G. Rius, J.-R. Huntzinger, A. Tiberj, N. Mestres, P. Godignon, and J. Camassel, Appl. Phys. Lett. **93**, 123503 (2008).

[14] W. A. de Heer, C. Berger, X. S. Wu, P. N. First, E. H. Conrad, X. B. Li, T. B. Li, M. Sprinkle, J. Hass, M. L. Sadowski, M. Potemski, and G. Martinez, Solid State Commun. **143**, 92 (2007).

[15] J. Hass, R. Feng, T. Li, X. Li, Z. Zong, W. A. de Heer, P. N. First, E. H. Conrad, C. A. Jeffrey, and C. Berger, Appl. Phys. Lett. **89**, 143106 (2006).

[16] J. Hass, R. Feng, J. E. Millan-Otoya, X. Li, M. Sprinkle, P. N. First, W. A. de Heer, E. H. Conrad, and C. Berger, Phys. Rev. B **75**, 214109 (2007).

[17] K. V. Emtsev, F. Speck, T. Seyller, L. Ley, and J. D. Riley, Phys. Rev. B **77**, 155303 (2008).

[18] F. Varchon, R. Feng, J. Hass, X. Li, B. N. Nguyen, C. Naud, P. Mallet, J. Y. Veuillen, C. Berger, E. H. Conrad, and L. Magaud, Phys. Rev. Lett. **99**, 126805 (2007).

[19] C. Berger, Z. M. Song, X. B. Li, X. S. Wu, N. Brown, C. Naud, D. Mayo, T. B. Li, J. Hass, A. N. Marchenkov, E. H. Conrad, P. N. First, and W. A. de Heer, Science **312**, 1191 (2006).

[20] M. Orlita, C. Faugeras, P. Plochocka, P. Neugebauer, G. Martinez, D. K. Maude, A. L. Barra, M. Sprinkle, C. Berger, W. A. de Heer, and M. Potemski, Phys. Rev. Lett. **101**, 267601 (2008).

[21] J. Hass, F. Varchon, J. E. Millan-Otoya, M. Sprinkle, N. Sharma, W. A. de Heer, C. Berger, P. N. First, L. Magaud, and E. H. Conrad, Phys. Rev. Lett. **100**, 125504 (2008).

[22] N. Camara, G. Rius, J.-R. Huntzinger, A. Tiberj, L. Magaud, N. Mestres, P. Godignon, and J. Camassel, Appl. Phys. Lett. **93**, 263102 (2008).

[23] http://www.novasic.com/

[24] C. Faugeras, A. Nerriere, M. Potemski, A. Mahmood, E. Dujardin, C. Berger, and W. A. de Heer, Appl. Phys. Lett. **92**, 011914 (2008).

[25] Z. G. Cambaz, G. Yushin, S. Osswald, V. Mochalin, and Y. Goyotsi, Carbon **46**, 841 (2008).

[26] J. Hass, W. A. de Heer, and E. H. Conrad, J. Phys.: Condens. Matter **20**, 323202 (2008).

[27] K. V. Vassilevski, N. G. Wright, I. P. Nikitina, A. B. Horsfall, A. G. O'Neill, M. J. Uren, K. P. Hilton, A. G. Masterton, A. J. Hydes, and C. M. Johnson, Semicond. Sci. Technol. **20**, 271 (2005).

[28] H. C. Jeong and J. D. Weeks, Phys. Rev. B **57**, 3939 (1998).

[29] D. J. Liu, J. D. Weeks, M. D. Johnson, and E. D. Williams, Phys. Rev. B **55**, 7653 (1997).

[30] D. S. L. Abergel, A. Russell, and V. I. Fal'ko, Appl. Phys. Lett. **91**, 063125 (2007).

[31] T. Stauber, N. M. R. Peres, and A. K. Geim, Phys. Rev. B **78**, 085432 (2008).

[32] R. R. Nair, P. Blake, A. N. Grigorenko, K. S. Novoselov, T. J. Booth, T. Stauber, N. M. R. Peres, and A. K. Geim, Science **320**, 1308 (2008).

[33] D. S. L. Abergel and V. I. Fal'ko, Phys. Rev. B **75**, 155430 (2007).

[34] A. C. Ferrari, J. C. Meyer, V. Scardaci, C. Casiraghi, M. Lazzeri, F. Mauri, S. Piscanec, D. Jiang, K. S. Novoselov, S. Roth, and A. K. Geim, Phys. Rev. Lett. **97**, 187401 (2006).

[35] D. Graf, F. Molitor, K. Ensslin, C. Stampfer, A. Jungen, C. Hierold, and L. Wirtz, Solid State Commun. **143**, 44 (2007).

[36] A. C. Ferrari, Solid State Commun. **143**, 47 (2007).

[37] C. Casiraghi, S. Pisana, K. S. Novoselov, A. K. Geim, and A. C. Ferrari, Appl. Phys. Lett. **91**, 233108 (2007).

[38] J. Yan, Y. B. Zhang, P. Kim, and A. Pinczuk, Phys. Rev. Lett. **98**, 166802 (2007).

[39] A. Gupta, G. Chen, P. Joshi, S. Tadigadapa, and P. C. Eklund, Nano Lett. **6**, 2667 (2006).

[40] A. Das, S. Pisana, B. Chakraborty, S. Piscanec, S. K. Saha, U. V. Waghmare, K. S. Novoselov, H. R. Krishnamurthy, A. K. Geim, A. C. Ferrari, and A. K. Sood, Nat. Nanotechnol. **3**, 210 (2008).

[41] Z. H. Ni, W. Chen, X. F. Fan, J. L. Kuo, T. Yu, A. T. S. Wee, and Z. X. Shen, Phys. Rev. B **77**, 115416 (2008).

[42] J. Rohrl, M. Hundhausen, K. V. Emtsev, S. Th, R. Graupner, and L. Ley, Appl. Phys. Lett. **92**, 201918 (2008).

[43] N. Ferralis, R. Maboudian, and C. Carraro, Phys. Rev. Lett. **101**, 156801 (2008).

[44] S. Latil, V. Meunier, and L. Henrard, Phys. Rev. B **76**, 201402 (2007).

[45] P. Poncharal, A. Ayari, T. Michel, and J. L. Sauvajol, Phys. Rev. B **78**, 113407 (2008).

[46] Z. H. Ni, Y. Y. Wang, T. Yu, Y. M. You, and Z. X. Shen, Phys. Rev. B **77**, 235403 (2008).